

High-Order Runge-Kutta Multiresolution Time Domain Methods for Computational Electromagnetics

Qunsheng Cao, Ramdev Kanapady, and Fernando Reitich

Abstract—In this paper we introduce a class of “Runge-Kutta Multi-Resolution Time Domain” (RK-MRTD) methods for problems of electromagnetic wave propagation that can attain an arbitrarily high order of convergence in both space and time. The methods capitalize on the high-order nature of spatial multi-resolution approximations by incorporating time-integrators with convergence properties that are commensurate with these. More precisely, the classical MRTD approach is adapted here to incorporate m th-order, m -stage, low storage Runge-Kutta methods for the time integration. As we show, if compactly supported wavelets of order N are used (e.g. the Daubechies D_N functions), and $m = N$ then the RK-MRTD methods deliver solutions which converge with this overall order; a variety of examples illustrate these properties. Moreover, we further show that the resulting algorithms are well-suited to parallel implementations, as we present results that demonstrate their near-optimal scaling.

Index Terms—Multiresolution time-domain (MRTD), wavelets, Runge-Kutta methods, high-order accuracy

I. INTRODUCTION

THE Multi-Resolution Time Domain (MRTD) method for the numerical simulation of solutions to Maxwell’s electromagnetic equations was initially introduced in [1] as an alternative to the popular and, by now, classical Finite-Difference Time Domain (FDTD) [2] approach. The basic idea behind MRTD is rather simple, as it reduces to a Method of Moments [3] (MoM) wherein the spatial basis functions are chosen from a multiresolution analysis [4]. This choice naturally results in the potential for highly resolved spatial variations of the fields. However, in typical implementations, the realization of this potential is hindered by a low-order (leap-frog) time stepping procedure. In this paper, we show how this limitation can be overcome by introducing a new class of MRTD schemes that incorporate high-order Runge-Kutta time integrators. We show that, with this addition, the resulting algorithms can be made to converge with arbitrarily high order in space and time, and that they consequently lead to more efficient simulations. Moreover, we demonstrate that these new numerical procedures retain the highly parallelizable characteristics of standard MRTD methods [5], [6] as we

present a variety of results from a fully-three dimensional parallel implementation.

The original developments of MRTD [1] highlighted an improvement in the observed dispersion characteristics over classical FDTD. Since then, a variety of studies have concentrated on the further analysis and application of these techniques, including the investigation of their stability, accuracy and dispersion properties (see e.g. [7]–[13]), the design of schemes for the incorporation of boundary and radiation conditions (e.g. [12], [14]–[16]), and the development of implementations for use in a variety of specific configurations [17]–[20]; the recent book [21] provides a good introduction to the subject.

The recent development of higher-order finite-difference schemes for electromagnetic applications (see e.g. [22]–[26]), on the other hand, has provided potential options over the classical FDTD scheme that are alternative to MRTD-based methodologies. Indeed, for instance, as noted in [27], the improved dispersion characteristics of MRTD techniques are attained at the cost of a larger stencil when compared to that of the Yee scheme [2] and, in fact, it results in solutions of a comparable quality to those produced by higher-order differencing schemes. The simplicity of implementation of standard as well as adaptive forms of MRTD procedures [13], [28]–[30], on the other hand, have continued to provide further impetus for the development of these methodologies. In fact, it is arguably these characteristics that account for the present popularity of the use of MRTD methods (e.g. over higher-order finite difference schemes) for tackling problems of practical relevance.

As we mentioned, our work provides a further step toward the attainment of “optimal” and widely applicable MRTD procedures for computational electromagnetics. Our results, originally announced in [31], are related to the concurrent work communicated in [32]. Both our and this latter work begin with the basic realization that the low-order time-integration strategy inherent in standard MRTD is rather contrary to their high spatial resolution. The work in [32], however, further advocates the use of a multi-resolution analysis (MRA) in time to circumvent this limitation. In contrast, our current work views the equations for the coefficients in the spatial multi-resolution expansion as satisfying a system of linear ordinary differential equations, to which some recently derived m th-order, m -stage, low storage Runge-Kutta methods for the time integration [33], [34] can be readily applied. We contend that this latter choice may be preferable over a space-time MRA [32] for a number of reasons. Most importantly, perhaps,

Manuscript received 23 January 2006; revised 5 May 2006.

Qunsheng Cao is with the College of Information Science & Technology, Nanjing University of Aeronautics and Astronautics, Nanjing, China.

Ramdev Kanapady is with the Department of Mechanical Engineering, University of Minnesota, Minneapolis, MN 55455, USA.

Fernando Reitich is with the School of Mathematics, University of Minnesota, Minneapolis, MN 55455, USA.

this approach automatically chooses a minimal stencil to attain an accuracy that is commensurate with the spatial resolution, and it does so with minimal storage requirements. In addition, as we explain in Section III-C, the implementation of the resulting scheme is rather straightforward, necessitating only the repeated application of “forward Euler” steps, and thus it can be readily used to upgrade existing MRTD implementations.

The rest of the paper is organized as follows: first in Section II we review the basic equations and concepts related to MRTD schemes; the classical method is introduced in Section II-A and its convergence properties are reviewed in Section II-B. Our new algorithms are then presented in Section III. The spatial discretization and its convergence properties are described in Sections III-A and III-B respectively; the time-integrator, in turn, is described in Section III-C. Numerical results that demonstrate the overall high-order accuracy of the resulting algorithm are presented in Section III-D. Section III-E is devoted to the stability and dispersion characteristics of the RK-MRTD procedures, and section III-F to their computational cost and memory requirements. In both cases, the properties of the new schemes are contrasted with those of standard MRTD methods, a comparison that further highlights the advantages of the proposed approach. Next, the details of the parallel implementation for the treatment of three-dimensional configurations are discussed in Section IV-A and results from this follow in Section IV-B. Finally, our conclusions are summarized in Section V.

II. ELECTROMAGNETICS AND MRTD

As we said, we shall be concerned with the numerical solution of the (time-domain) Maxwell equations

$$\nabla \times \mathbf{E} = -\frac{\partial \mathbf{B}}{\partial t} \quad (1a)$$

$$\nabla \times \mathbf{H} = \mathbf{J} + \frac{\partial \mathbf{D}}{\partial t} \quad (1b)$$

$$\nabla \cdot \mathbf{D} = 0 \quad (1c)$$

$$\nabla \cdot \mathbf{B} = 0. \quad (1d)$$

where \mathbf{E} , \mathbf{H} , \mathbf{D} , \mathbf{B} , \mathbf{J} are the electric field, the magnetic field, the electric displacement, the magnetic induction and the current, respectively. We shall assume that the media are linear

$$\mathbf{D} = \varepsilon \mathbf{E}$$

$$\mathbf{B} = \mu \mathbf{H}$$

$$\mathbf{J} = \sigma \mathbf{E}$$

and will consider both initial-value problems, wherein initial conditions

$$\mathbf{E}(x, 0) = \mathbf{E}_0(x), \quad \mathbf{H}(x, 0) = \mathbf{H}_0(x)$$

are prescribed, and scattering problems where an unknown scattered field (\mathbf{E}^{scat} , \mathbf{H}^{scat}) arises in response to incident radiation (\mathbf{E}^{inc} , \mathbf{H}^{inc}) in such a way that the total field

$$\mathbf{E}^{\text{total}} = \mathbf{E} = \mathbf{E}^{\text{inc}} + \mathbf{E}^{\text{scat}}$$

$$\mathbf{H}^{\text{total}} = \mathbf{H} = \mathbf{H}^{\text{inc}} + \mathbf{H}^{\text{scat}}$$

satisfies equations (1). At material interfaces, the tangential components of the (total) electromagnetic field must be continuous

$$\mathbf{n} \times (\mathbf{E}^+ - \mathbf{E}^-) = 0, \quad \mathbf{n} \times (\mathbf{H}^+ - \mathbf{H}^-) = 0$$

where \mathbf{n} denotes the normal vector to the interface and “ \pm ” denotes the limiting values from either side of the corresponding quantity. In the limiting case of a perfect electric conductor (PEC) these conditions reduce to

$$\mathbf{n} \times \mathbf{E}^+ = 0.$$

A. Multi-Resolution Time Domain (MRTD) Method

The original MRTD scheme [1] is based on a spatial multi-resolution representation of the fields at each instant in time. For instance if, for simplicity, only scaling functions are used (“S-MRTD” [1]), this representation takes on the form

$$E_x(x, y, z, t) = \sum_{n,i,j,k=-\infty}^{+\infty} \phi_x E_{i+\frac{1}{2},j,k}^n h_n(t) \phi_{i+\frac{1}{2}}(x) \phi_j(y) \phi_k(z) \quad (2a)$$

$$E_y(x, y, z, t) = \sum_{n,i,j,k=-\infty}^{+\infty} \phi_y E_{i,j+\frac{1}{2},k}^n h_n(t) \phi_i(x) \phi_{j+\frac{1}{2}}(y) \phi_k(z) \quad (2b)$$

$$E_z(x, y, z, t) = \sum_{n,i,j,k=-\infty}^{+\infty} \phi_z E_{i,j,k+\frac{1}{2}}^n h_n(t) \phi_i(x) \phi_j(y) \phi_{k+\frac{1}{2}}(z) \quad (2c)$$

$$H_x(x, y, z, t) = \sum_{n,i,j,k=-\infty}^{+\infty} \phi_x H_{i+\frac{1}{2},j,k}^{n+\frac{1}{2}} h_{n+\frac{1}{2}}(t) \phi_i(x) \phi_{j+\frac{1}{2}}(y) \phi_{k+\frac{1}{2}}(z) \quad (2d)$$

$$H_y(x, y, z, t) = \sum_{n,i,j,k=-\infty}^{+\infty} \phi_y H_{i,j+\frac{1}{2},k}^{n+\frac{1}{2}} h_{n+\frac{1}{2}}(t) \phi_{i+\frac{1}{2}}(x) \phi_j(y) \phi_{k+\frac{1}{2}}(z) \quad (2e)$$

$$H_z(x, y, z, t) = \sum_{n,i,j,k=-\infty}^{+\infty} \phi_z H_{i,j,k+\frac{1}{2}}^{n+\frac{1}{2}} h_{n+\frac{1}{2}}(t) \phi_{i+\frac{1}{2}}(x) \phi_{j+\frac{1}{2}}(y) \phi_k(z) \quad (2f)$$

where $\phi_v E_{i,j,k}^n$ and $\phi_v H_{i,j,k}^n$, $v = x, y, z$, are the (constant, unknown) field expansion coefficients. Here the function ϕ is the *scaling function*,

$$\phi_l(v) = \phi\left(\frac{v}{\Delta v} - l\right) \quad \text{for } v = x, y, z,$$

$h(t)$ is the “impulse function”

$$h(t) = \begin{cases} 1 & \text{if } |t| < 1/2, \\ 1/2 & \text{if } |t| = 1/2, \\ 0 & \text{if } |t| > 1/2, \end{cases}$$

and

$$h_l(t) = h\left(\frac{t}{\Delta t} - l\right). \quad (3)$$

The update equations then follow from the relations

$$\int_{-\infty}^{+\infty} h_i(t) h_j(t) dt = \delta_{i,j} \Delta t \quad (4a)$$

$$\int_{-\infty}^{+\infty} h_i(t) \frac{\partial h_{j+\frac{1}{2}}(t)}{\partial t} dt = \delta_{i,j} - \delta_{i,j+1} \quad (4b)$$

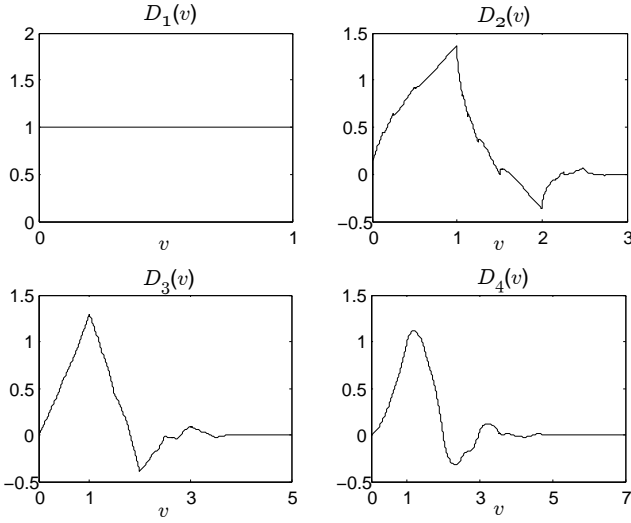


Fig. 1. The Daubechies scaling functions D_N , $N = 1, 2, 3$ and 4 .

$$\int_{-\infty}^{+\infty} \phi_i(v)\phi_j(v) dv = \delta_{i,j}\Delta v \quad (4c)$$

$$\int_{-\infty}^{+\infty} \phi_i(v)\frac{\partial\phi_{j+\frac{1}{2}}(v)}{\partial v}dv = \sum_{\nu=-\infty}^{+\infty} a(\nu)\delta_{i+\nu,j} \quad (4d)$$

upon substituting the expansions (2) into (1) and integrating against $\phi_i(v)$, $v = x, y, z$, and $h_l(t)$. The non-zero coefficients $a(\nu)$ are shown in Table I for the cases of the Daubechies scaling functions D_2 through D_4 (see Figure 1).

TABLE I
THE NON-ZERO COEFFICIENTS $a(\nu)$ FOR THE DAUBECHIES SCALING FUNCTIONS D_2 THROUGH D_4 .

D_2		D_3		D_4	
ν	$a(\nu)$	ν	$a(\nu)$	ν	$a(\nu)$
0	-0.0104166667	0	-0.0000080265	0	0.0000000041
1	0.0937500000	1	0.0034701413	1	-0.0000108999
2	-1.2291666667	2	-0.0287617723	2	-0.0008308695
3	1.2291666666	3	0.1371343465	3	0.0086543236
4	-0.0937500000	4	-1.2918129281	4	-0.0419957460
5	0.0104166667	5	1.2918129281	5	0.1560100710
		6	-0.1371343465	6	-1.3110340773
		7	0.0287617723	7	1.3110340773
		8	-0.0034701413	8	-0.1560100710
		9	0.0000080265	9	0.0419957460
				10	-0.0086543236
				11	0.0008308695
				12	0.0000108999
				13	-0.0000000041

Explicitly, in a region of constant material properties, the resulting scheme takes on the form ($\sigma = 0$)

$$\phi_x E_{i+\frac{1}{2},j,k}^{n+1} = \phi_x E_{i+\frac{1}{2},j,k}^n \quad (5a)$$

$$+ \frac{1}{\varepsilon} \sum_{\nu} a(\nu) \left(\phi_z H_{i+\frac{1}{2},j+\nu+\frac{1}{2},k}^{n+\frac{1}{2}} \frac{\Delta t}{\Delta y} - \phi_y H_{i+\frac{1}{2},j,k+\nu+\frac{1}{2}}^{n+\frac{1}{2}} \frac{\Delta t}{\Delta z} \right)$$

$$\phi_x H_{i,j+\frac{1}{2},k+\frac{1}{2}}^{n+\frac{1}{2}} = \phi_x H_{i,j+\frac{1}{2},k+\frac{1}{2}}^{n-\frac{1}{2}} \quad (5b)$$

$$+ \frac{1}{\mu} \sum_{\nu} a(\nu) \left(\phi_y E_{i,j+\frac{1}{2},k+\nu+1}^n \frac{\Delta t}{\Delta z} - \phi_z E_{i,j+\nu+1,k+\frac{1}{2}}^n \frac{\Delta t}{\Delta y} \right)$$

and similarly for the remaining components of the electromagnetic field. A geometrical interpretation of the staggered approximation (5) is given in Figure 2.

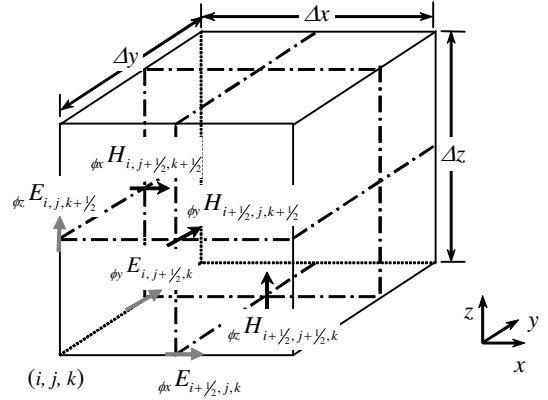


Fig. 2. Geometrical representation of the classical MRTD discretization.

B. Convergence of MRTD solutions

As it follows from the decomposition (2) the standard MRTD scheme is highly accurate in the spatial description of the fields. The use of the impulse functions (3) and the staggered approximations (see Figure 2), however, limit its accuracy to second order, much as in the classical FDTD scheme.

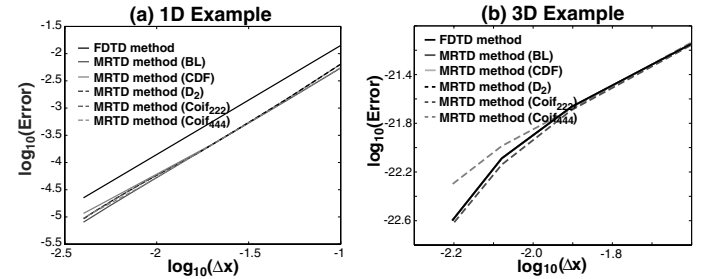


Fig. 3. Convergence of the classical MRTD and FDTD schemes.

An example of the effect of these limitations is provided in Figure 3. There we display the results corresponding to one- and three-dimensional examples wherein a compactly supported pulse propagates in free space. More precisely, in one space dimension, Maxwell's equations reduce to (cf. (1))

$$\varepsilon \partial_t E - \partial_x H = 0 \quad (6a)$$

$$\mu \partial_t H - \partial_x E = 0 \quad (6b)$$

where (E, H) are the transverse components of the total electromagnetic field. The propagation of a pulse $u = u(x)$ in free space ($c = (\mu\varepsilon)^{-1/2} = 1$ in dimensionless form) can be simulated, in this context, by imposing exact radiation conditions at the boundary of the computational domain.

Indeed, in one space dimension, these conditions take on the simple (local) form

$$E + H = 0 \quad \text{at } x = a \quad (7a)$$

$$E - H = 2u(x - t) \quad \text{at } x = -a. \quad (7b)$$

The example in Figure 3 corresponds to a smooth, compactly supported pulse with an initial form

$$E(x, t = 0) = u(x), \quad x \in (-a, a) \quad (8a)$$

$$H(x, t = 0) = -u(x), \quad x \in (-a, a) \quad (8b)$$

where

$$u(x) = w\left(\frac{x + b}{\delta}\right), \quad (9)$$

$$w(y) = \begin{cases} (y - 1)^{10}(y + 1)^{10} & \text{for } |y| < 1 \\ 0 & \text{otherwise} \end{cases} \quad (10)$$

and $a = 12$, $b = 0$ and $\delta = 1$ (see Figure 4).

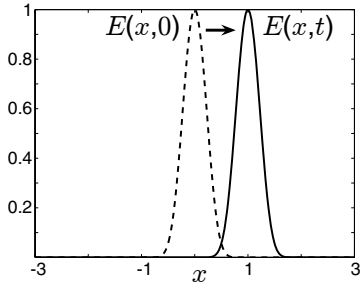


Fig. 4. Solution to the one-dimensional problem corresponding to the results in Figure 3(a).

In this case, of course, the exact solution is simply given by

$$\begin{aligned} E^{\text{exact}}(x, t) &= u(x - t) \\ H^{\text{exact}}(x, t) &= -u(x - t). \end{aligned}$$

Similar considerations apply to a spherical pulse propagating in three-dimensions. The results in Figure 3 correspond to the mean squared error over the support of the pulse at time $t = 1$. Note that the order of convergence is approximately equal to two, regardless of the specific wavelet basis chosen for the simulation.

III. RUNGE-KUTTA MULTI-RESOLUTION TIME DOMAIN (RK-MRTD) METHOD

In this section we present the details of our new algorithm. First in Section III-A we describe the wavelet expansion that we use for the spatial discretization; in Section III-B we recall the convergence properties of these expansions and we motivate the need to incorporate a higher order time integrator. One such scheme is presented in Section III-C, and numerical results that confirm the attainment of an overall order of convergence that respects the spatial resolution are shown in Section III-D. Moreover, the stability and dispersive characteristics of the methods are discussed in Section III-E and, finally, their computational cost is analyzed in Section III-F. In both cases, as we mentioned, we contrast these characteristics

with those of standard MRTD implementations, and we show that the enhanced accuracy of the new procedures translates, in fact, in higher quality solutions and lower computational times.

A. Spatial discretization

The expansion of the fields that we shall use is largely as that in equations (2) in Section II-A, except for the use of impulse functions in time. Instead, we let the actual wavelet coefficients be *functions* of this variable, which are to be determined. More precisely, we let

$$E_x(x, y, z, t) = \sum_{i,j,k=-\infty}^{+\infty} \phi_x E_{i+\frac{1}{2},j,k}(t) \phi_{i+\frac{1}{2}}(x) \phi_j(y) \phi_k(z) \quad (11a)$$

$$E_y(x, y, z, t) = \sum_{i,j,k=-\infty}^{+\infty} \phi_y E_{i,j+\frac{1}{2},k}(t) \phi_i(x) \phi_{j+\frac{1}{2}}(y) \phi_k(z) \quad (11b)$$

$$E_z(x, y, z, t) = \sum_{i,j,k=-\infty}^{+\infty} \phi_z E_{i,j,k+\frac{1}{2}}(t) \phi_i(x) \phi_j(y) \phi_{k+\frac{1}{2}}(z) \quad (11c)$$

$$H_x(x, y, z, t) = \sum_{i,j,k=-\infty}^{+\infty} \phi_x H_{i+\frac{1}{2},j,k}(t) \phi_i(x) \phi_{j+\frac{1}{2}}(y) \phi_{k+\frac{1}{2}}(z) \quad (11d)$$

$$H_y(x, y, z, t) = \sum_{i,j,k=-\infty}^{+\infty} \phi_y H_{i,j+\frac{1}{2},k}(t) \phi_{i+\frac{1}{2}}(x) \phi_j(y) \phi_{k+\frac{1}{2}}(z) \quad (11e)$$

$$H_z(x, y, z, t) = \sum_{i,j,k=-\infty}^{+\infty} \phi_z H_{i,j,k+\frac{1}{2}}(t) \phi_{i+\frac{1}{2}}(x) \phi_{j+\frac{1}{2}}(y) \phi_k(z) \quad (11f)$$

and derive the equations

$$\frac{\partial \phi_x E_{i+\frac{1}{2},j,k}(t)}{\partial t} = \frac{1}{\epsilon} \times \quad (12a)$$

$$\sum_{\nu} a(\nu) \left(\phi_x H_{i+\frac{1}{2},j+\nu+\frac{1}{2},k}(t) \frac{1}{\Delta y} - \phi_y H_{i+\frac{1}{2},j,k+\nu+\frac{1}{2}}(t) \frac{1}{\Delta z} \right) \quad (12b)$$

$$\frac{\partial \phi_x H_{i,j+\frac{1}{2},k+\frac{1}{2}}(t)}{\partial t} = \frac{1}{\mu} \times$$

$$\sum_{\nu} a(\nu) \left(\phi_y E_{i,j+\frac{1}{2},k+\nu+1}(t) \frac{1}{\Delta z} - \phi_z E_{i,j+\nu+1,k+\frac{1}{2}}(t) \frac{1}{\Delta y} \right)$$

analogous to (5).

B. Convergence in space

As we stated, the use of a spatial multi-resolution analysis (or simply that of appropriate scaling functions) provides the potential for accurate spatial representations, which may converge with high order. The basic reason can be traced to a rather fundamental result (see e.g. [35]) which states that the following are equivalent properties for any integer p :

- Smooth functions can be approximated with error $O(\Delta x^p)$ at every scale $\Delta x = 2^{-j}$, that is

$$\|f - \sum c_k \phi\left(\frac{x}{\Delta x} - k\right)\| \leq C(\Delta x)^p \|f^{(p)}\|$$

for suitable c_k ($c_k \Delta x = \int f(x) \phi(\frac{x}{\Delta x} - k) dx$ for orthonormal families, cf. (4c));

- The polynomials $\{1, x, \dots, x^{p-1}\}$ are linear combinations of the translates $\phi(x - k)$;
- The first p moments of the wavelet ψ vanish

$$\int x^m \psi(x) dx = 0 \quad \text{for } m = 0, 1, \dots, p-1; \text{ and}$$

- The wavelet coefficients of a smooth function decay as

$$\int f(x) \psi\left(\frac{x}{\Delta x}\right) dx \leq C(\Delta x)^p.$$

For the Daubechies scaling functions D_N , for instance, we have $p = N$ [35]. As a result the spatial representation of any (smooth) function in terms of these (cf. (11)) converges with order N ; see Figure 5.

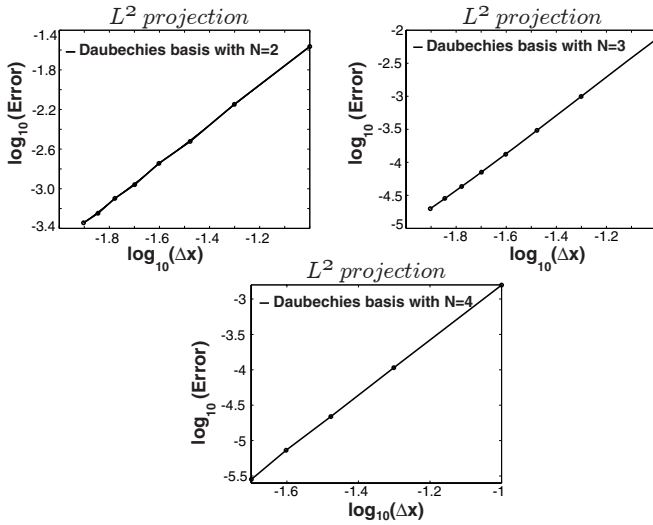


Fig. 5. Convergence of the projection onto the span of the scaling functions at varying scales Δx . The order of convergence of the projection is two, three and four when using D_2 , D_3 and D_4 respectively.

This high-order convergence, however, is limited in standard MRTD implementations by the low (second) order time integration strategy and the choice

$$\Delta t = \alpha \frac{\Delta x}{c} \quad (\alpha \leq 1) \quad (13)$$

to satisfy the CFL stability condition. Indeed, with this choice, the overall error is bounded by

$$\begin{aligned} \text{MRTD Error} &\leq A \Delta x^N + B \Delta t^2 \leq A \Delta x^N + B \left(\alpha \frac{\Delta x}{c} \right)^2 \\ &\leq C \Delta x^2 \end{aligned} \quad (14)$$

and thus limited to second order. This estimate is confirmed in Figure 6 where we further show that the higher spatial order can be recovered in the overall solution by simply setting

$$\Delta t = \alpha \frac{\Delta x^p}{c}$$

with $p > 1$. More precisely, in these figures we show that fourth and sixth order can be attained in space-time using, for instance, the Battle-Lemarie scaling functions and time steps proportional to Δx^2 and Δx^3 respectively.

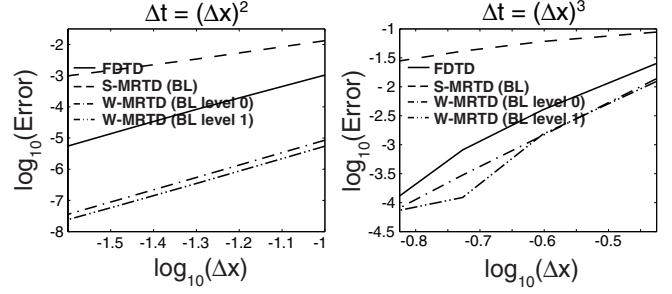


Fig. 6. Convergence of the MRTD approach for time-steps of order $(\Delta x)^2$ and $(\Delta x)^3$. Note that the order of convergence for the MRTD results on the left and right panels are approximately four and six, respectively.

C. Higher order time integration

The system of ordinary differential equations (12) (and its version for the remaining components of the field) can be symbolically written as

$$\begin{aligned} \frac{\partial \mathbf{E}^\phi}{\partial t} &= \mathbf{L}_H \mathbf{H}^\phi \\ \frac{\partial \mathbf{H}^\phi}{\partial t} &= \mathbf{L}_E \mathbf{E}^\phi \end{aligned}$$

If sources are included, then the system can be put into the form

$$\frac{\partial \mathbf{F}}{\partial t} = \mathbf{L} \mathbf{F} + \mathbf{S}(t) \quad (15)$$

where

$$\mathbf{F} = \begin{Bmatrix} \mathbf{E}^\phi \\ \mathbf{H}^\phi \end{Bmatrix}$$

and

$$\mathbf{L} = \begin{bmatrix} \mathbf{0} & \mathbf{L}_H \\ \mathbf{L}_E & \mathbf{0} \end{bmatrix}.$$

To achieve the same order of convergence as that in Figure 6 without resorting to unduly small time steps, we propose to discretize the system (15) with an m th-order, m -stage, strong stability preserving Runge-Kutta (SSP-RK) with low storage requirements. The scheme, originally introduced in [33] for homogeneous systems and extended to systems such as (15) in [34] has the form

$$\begin{aligned} \mathbf{F}^{(0)} &= \mathbf{F}_n \\ \mathbf{F}^{(i)} &= \mathbf{F}^{(i-1)} + \Delta t \mathbf{L} \mathbf{F}^{(i-1)} + \Delta t \mathbf{S}^{(i)}, \quad i = 1, \dots, m \\ \mathbf{F}_{n+1} &= \sum_{k=0}^m \alpha_{m,k} \mathbf{F}^{(k)} \end{aligned} \quad (16)$$

where

$$\mathbf{F}_n = \mathbf{F}(t_n),$$

$$\mathbf{S}^{(i)} = \left(I + \Delta t \frac{\partial}{\partial t} \right)^{i-1} \mathbf{S}(t_n)$$

and I denotes the identity operator. The coefficients $\alpha_{m,k}$ are given by [33], [34]

$$\begin{aligned}\alpha_{1,0} &= 1 \\ \alpha_{m,k} &= \frac{1}{k} \alpha_{m-1,k-1}, \quad k = 1, \dots, m-2, \\ \alpha_{m,m} &= \frac{1}{m!}, \quad \alpha_{m,m-1} = 0, \quad \alpha_{m,0} = 1 - \sum_{k=1}^m \alpha_{m,k}.\end{aligned}$$

D. Convergence in space-time

In this section, we present results that confirm the expected rate of convergence of the RK-MRTD approach. To this end, we evaluate the errors incurred by the approximation of the problem described in equations (6)-(10). The expansion coefficients $E_i(t=0)$ and $H_i(t=0)$ for the initial data in (8) are computed by projecting onto the corresponding set of scaling functions (D_N , $N = 2, 3, 4$), i.e.

$$E(x, 0) = \sum_i E_i(0) \phi_i(x);$$

(see Section III-B), and the error is measured in the mean square

$$\text{RK-MRTD } L^2\text{-error} = \left(\sum_i (E_i^{\text{exact}} - E_i)^2 \Delta x \right)^{\frac{1}{2}}.$$

These errors and respective estimates of convergence orders are presented in Table II. The results demonstrate that a uniform overall order can be attained with the use of the proposed scheme. This, of course, results from the easily derivable estimate

$$\text{RK-MRTD } L^2\text{-error} \leq C_x \Delta x^N + C_t \Delta t^m \quad (17)$$

which, for reasons of stability, holds provided (13) is satisfied for a suitable CFL constant α (see section III-E).

We also note that these results, together with (13), demonstrate that high-order convergence can be achieved with time steps whose size is just *linearly proportional* to that of the spatial discretization (compare with Figure 6). Moreover, the last sub-table provides further evidence that a refinement in space (e.g. using the —fourth order— scaling function D_4) does not translate into significant gains if not accompanied by a commensurate treatment of the time variable. In fact, as it follows from (17), if (13) holds then the overall order p of the algorithm can be summarized as

$$p = \min(m, N).$$

In particular, if $m = N$, then

$$\text{RK-MRTD } L^2\text{-error} \leq C_N \Delta x^N. \quad (18)$$

E. Dispersion and stability

As we have argued, the use of RK-MRTD schemes can be extremely beneficial from an accuracy standpoint. And this, of course, translates, in particular, into a more accurate satisfaction of the exact dispersion relation by the corresponding numerical solutions; see e.g. [36]. An example of this is

TABLE II
CONVERGENCE OF RK-MRTD FOR DIFFERENT VALUES OF m AND N .

D_2 ; SSP-RK2		
Δx	L^2 -error	Order
1.000000e-01	3.342552e-02	
3.333333e-02	3.436956e-03	2.07
2.000000e-02	1.217792e-03	2.03
1.428571e-02	6.170588e-04	2.02
1.111111e-02	3.717976e-04	2.02

D_3 ; SSP-RK3		
Δx	L^2 -error	Order
1.000000e-01	6.746640e-03	
3.333333e-02	2.911401e-04	2.86
2.000000e-02	6.352483e-05	2.98
1.428571e-02	2.321555e-05	2.99
1.111111e-02	1.094003e-05	2.99

D_4 ; SSP-RK4		
Δx	L^2 -error	Order
1.000000e-01	2.054775e-03	
3.333333e-02	2.641036e-05	3.96
2.000000e-02	3.277183e-06	4.09
1.428571e-02	8.300989e-07	4.08
1.111111e-02	3.020184e-07	4.02

D_4 ; SSP-RK2		
Δx	L^2 -error	Order
1.000000e-01	1.214359e-03	
3.333333e-02	1.442995e-04	1.94
2.000000e-02	5.307721e-05	1.96
1.428571e-02	2.723436e-05	1.98
1.111111e-02	1.653033e-05	1.99

TABLE III
CFL NUMBERS FOR RK-MRTD

$N = m$	α
2	0.50
3	0.33
4	0.25

presented in Fig. 7 where we have plotted the result of a long-time propagation experiment for the pulse in Fig. 4. While almost no dissipation is visible in any of the implementations, the effects of dispersion are rather pronounced for $N = m = 2$. These effects get mollified when we set $N = m = 3$; when $N = m = 4$ the approximate solution is almost indistinguishable from the exact solution.

However, these significant accuracy gains are obtained at a cost of a more stringent stability requirement [37]. Indeed, the result of some simple numerical experiments demonstrate that, for the RK-MRTD methods introduced here, the maximal time step for which the method remains stable is inversely proportional to m ; see Table III. Within a typical simulation, these requirements, of course, translate into the need to effect a larger number of time steps. As we explain below, however, these additional demands are largely compensated for by the higher space-time accuracy, resulting in an *overall* computational effort to attain any given accuracy that can be substantially lower than that required by standard MRTD implementations.

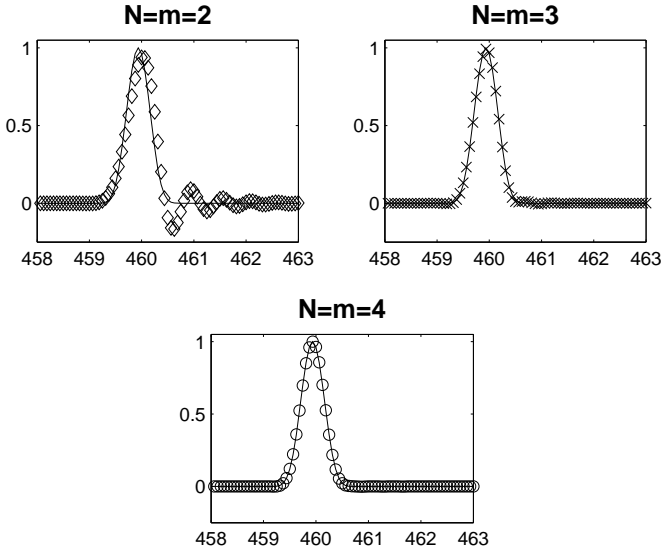


Fig. 7. Long-time evolution of the pulse in Fig. 4 using the RK-MRTD scheme with $N = m = 2, 3, 4$. For reference, the solid line depicts the exact solution.

F. Computational cost and memory requirements

In this section we discuss the computational cost and memory requirements of our new numerical procedures, and we contrast them with those of classical MRTD. The issue of memory, in fact, is rather simple: if the values of the fields are needed for a period of time, then the memory requirements are the same, as the time-series of the fields needs to be stored in both cases. If, however, only the fields at a final time are of interest, the memory needs of the new schemes are twice that of the standard MRTD. Indeed, while for the latter only the values of \mathbf{E}^n and $\mathbf{H}^{n-1/2}$ (cf. (5)) need to be stored at each time step, the RK-MRTD procedure demands that both $\mathbf{F}^{(i)}$ and \mathbf{F}_{n+1} (cf. (16)) be stored as the latter is evaluated.

The issue of computational cost, on the other hand, is a bit more subtle. For a single time step, the cost (number of operations) of standard MRTD is (cf. (5))

$$\begin{aligned} \text{MRTD Cost Per Time Step} &= 2 \times (\text{Nr. of grid points}) \\ &\times (\text{Size of stencil}) = 2(n_2)^d(4N - 2), \end{aligned} \quad (19)$$

if the scaling function D_N is used. Here d is the number of dimensions (1, 2 or 3) and n_2 denotes the number of points in a single direction, that is,

$$n_2 = \frac{1}{\Delta x_2} \quad (20)$$

for a domain of unit size, where Δx_2 denotes the grid spacing. The RK-MRTD scheme, on the other hand, demands that for each time step we perform m stages in which we must

1. evaluate $\mathbf{L}\mathbf{F}^{(i-1)}$; and
2. add the result \mathbf{F}_{n+1} .

Clearly, step 1 costs $2(n_m)^d(4N - 2)$ operations, while step 2 involves $2(n_m)^d$, where

$$n_m = \frac{1}{\Delta x_m} \quad (21)$$

and Δx_m is the grid spacing for the order- m method. As a result, a single time step of the RK-MRTD procedure calls for

$$\text{RK-MRTD Cost Per Time Step} = 2(n_m)^d m(4N - 1).$$

In particular, if $m = N$ (cf. Table II), we have

$$\text{RK-MRTD Cost Per Time Step} = 2(n_N)^d N(4N - 1). \quad (22)$$

On the other hand, as described in section III-E, if Δt_2 denotes the maximal stable time-step for MRTD, the time step Δt_N for RK-MRTD ($m = N$) must be chosen as

$$\Delta t_N = \frac{2\Delta t_2}{N}$$

Collecting these results, we obtain

$$\text{MRTD Cost to time 1} = 2(n_2)^d(4N - 2)\frac{1}{\Delta t_2} \quad (23)$$

and

$$\text{RK-MRTD } (m = N) \text{ Cost to time 1} \quad (24)$$

$$\begin{aligned} &= 2(n_N)^d N(4N - 1)\frac{1}{\Delta t_N} \\ &= (n_N)^d(4N - 1)N^2\frac{1}{\Delta t_2}. \end{aligned} \quad (25)$$

In order to compare the efficiency of these alternative schemes we must now choose appropriate values of n_2 and n_N . It is here then where the higher order convergence properties of RK-MRTD manifest themselves as, for any given accuracy, a larger grid spacing can be taken when compared to that required by standard MRTD. Indeed, the estimates (14) and (18) suggest that similar accuracies between standard (second-order accurate) MRTD and higher order RK-MRTD evaluations should be attainable provided

$$\frac{\Delta x_2}{(\Delta x_N)^{N/2}} = Q_{d,N} \quad (26)$$

for some constants $Q_{d,N}$, depending *only* on the dimension and on the order of approximation (i.e. independent of the grid spacing). Using (20), (21) and (26) we conclude that comparable errors can be obtained provided

$$n_N = (Q_{d,N}n_2)^{2/N}.$$

Then, from (24) we get

$$\begin{aligned} \text{RK-MRTD } (m = N) \text{ Cost for a given accuracy} &= (Q_{d,N}n_2)^{(2d)/N} (4N - 1)N^2\frac{1}{\Delta t_2} \\ &= \left(2(n_2)^d(4N - 2)\frac{1}{\Delta t_2}\right) \\ &\times (Q_{d,N})^{(2d)/N} n_2^{-(1-2/N)d}\frac{(4N - 1)N^2}{2(4N - 2)} \\ &< \gamma \times (\text{MRTD Cost for the same accuracy}) \end{aligned}$$

provided

$$\left(\frac{Q_{d,N}}{(n_2)^{N/2-1}}\right)^{(2d)/N} \frac{(4N - 1)N^2}{2(4N - 2)} < \gamma. \quad (27)$$

The key feature of equation (27) is, of course, that the first ratio in the left-hand side can be made arbitrarily small as the

number of points in a single direction is increased. Moreover, this ratio is raised to a power that increases with increasing dimension, providing a further mechanism for the reduction of the magnitude of the left-hand side. To provide a numerical example, we consider the most unfavorable case of the one dimensional example of Table II. In Fig. 8 we have plotted

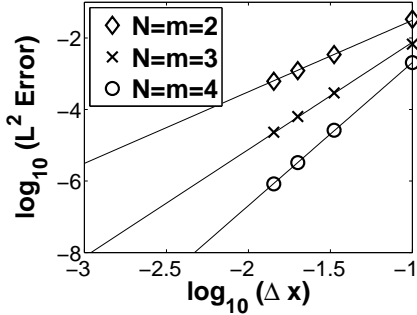


Fig. 8. Log-log plot of the errors from table II, and best fits to lines with slopes given by the order of the method.

the results in this table in logarithmic scales, together with the best linear fits to the data that have slopes prescribed by the order of convergence ($m = N$). These plots clearly convey the effect of higher order convergence and, moreover, the linear fits allow us to extrapolate to a plot of the necessary grid spacing to attain any given accuracy, by simply interchanging the axes; see Fig. 9(a). From this, in turn, the constants $Q_{1,N}$

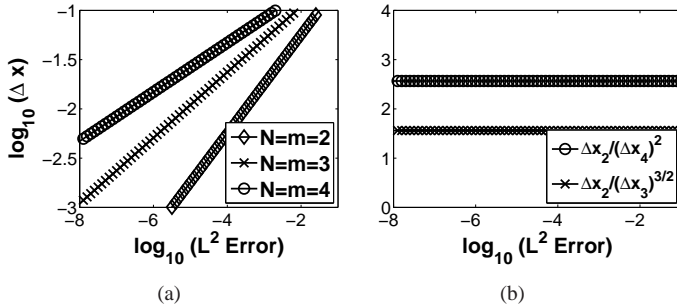


Fig. 9. (a) Log-log plot of the size of the spatial grid as a function of the desired accuracy (“ L^2 Error”; from Fig. 8). (b) Values of the quotients $\Delta x_2/(\Delta x_3)^{3/2}$ and $\Delta x_2/(\Delta x_4)^2$ as functions of the desired accuracy, as derived from the left plot.

in (26) can be estimated by equating the error in standard MRTD to that of $m = N = 2$ and evaluating the quotients in the left-hand side of (26). The results of this exercise are displayed in Fig. 9(b) which shows that, for $N = 3, 4$,

$$Q_{1,N} = \frac{2N - 3}{2}. \quad (28)$$

In these cases then, equation (27) translates to

$$\frac{6.49}{n_2^{1/3}} < \gamma \quad \text{if } N = 3$$

and

$$\frac{13.55}{n_2^{1/2}} < \gamma \quad \text{if } N = 4.$$

Letting $\gamma = 1$ we obtain that the cost of RK-MRTD is less than that of standard MRTD provided

$$n_2 > \begin{cases} 272, & \text{if } N = 3, \\ 183, & \text{if } N = 4. \end{cases}$$

Similarly, if $\gamma < 1/2$, equation (27) implies that the cost is *half* that of standard MRTD if

$$n_2 > \begin{cases} 2183, & \text{if } N = 3, \\ 734, & \text{if } N = 4. \end{cases}$$

IV. PARALLEL IMPLEMENTATION AND RESULTS

In this section we present performance results for a parallel implementation of the RK-MRTD formulation. The details of the implementation are first reviewed in Section IV-A. Then, in Section IV-B we present some speed-up results that highlight the almost optimal scalability of the algorithm.

A. Parallel implementation

The implementation is based on “coarse grained parallelization” using the Message Passing Interface (MPI). We recall that coarse grained parallelization is based on a division of the computational domain into subdomains which are mapped onto individual processors. In general, the parallel performance of the algorithm depends on the parallel overhead, which is mainly a function of the collective communication overhead between processors and the communication between neighboring processors. Since the method is based on explicit time discretizations, the communication overhead is restricted to nearest neighbors.

B. Numerical examples

The parallel performance of the implementation on an IBM SP parallel machine is illustrated in Figures 10 and 12. Figure 10 corresponds to parallel implementations of the one-dimensional example in (6)-(10), showing almost optimal speed-up with decreasing grid spacing.

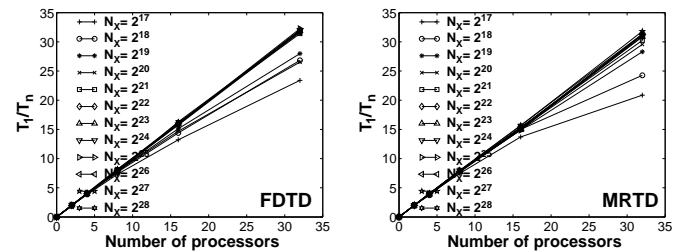


Fig. 10. Parallel speedup for a one-dimensional example of application of the RK-MRTD formulation.

The three-dimensional example in Figure 12, on the other hand, corresponds to a simple scattering problem for a hexahedral PEC as depicted in Figure 11. The scatterer, with dimensions $10\text{m} \times 30\text{m} \times 10\text{m}$, is illuminated by a Gaussian pulse at $\theta^{\text{inc}} = 90^\circ$, $\phi^{\text{inc}} = 90^\circ$ and $\psi^{\text{inc}} = 45^\circ$ with increasing center frequencies from 5MHz to 10MHz. A Perfectly Matched Layer (PML) is used to truncate the computational domain as shown in Figure 11. Figure 12 shows a parallel speed-up which is, again, close to ideal as the number of degrees of freedom is increased.

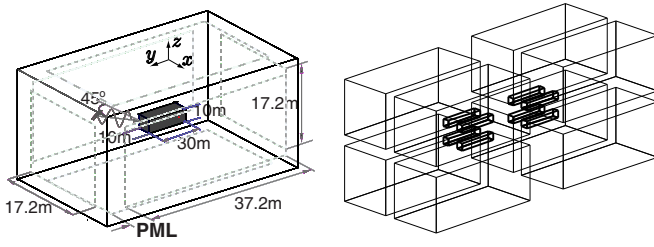


Fig. 11. Problem description for the parallel performance study of the RK-MRTD formulation, and schematic of subdomain partitioning.

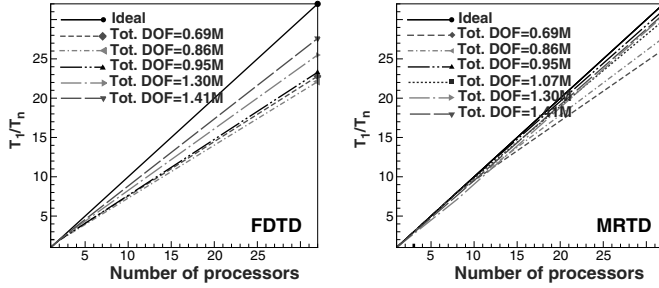


Fig. 12. Parallel speedup for a three-dimensional example (see Figure 11) of application of the RK-MRTD formulation.

V. CONCLUSIONS

In this paper we have presented a new method for the numerical simulation of electromagnetic wave propagation that is based on the classical MRTD procedure. The basic premise relies on the observation that this scheme produces high-order accurate approximations in space, to which, for instance, its improved dispersion characteristics over the standard finite-difference method (FDTD) can actually be attributed. As we have shown, however, the high quality of the spatial approximations in standard MRTD is severely impaired by the typical leap-frog time-integrator associated with it. A possible remedy could rely on the use of much reduced time steps to bring the time-integration error in line with that of the spatial approximations (cf. Figure 6), or on the use of space-time MRA [32]. Here, in contrast, we propose a significantly more efficient strategy that relies on the replacement of the second-order leap-frog scheme with a high-order Runge-Kutta procedure to approximate the time evolution while retaining the accurate multi-resolution treatment in space. We demonstrated that the resulting method provides solutions wherein the errors from both discretizations are comparable and, thus, that it realizes the full potential of spatial multi-resolution decompositions. Moreover, we have also shown that the enhanced accuracy of the new numerical schemes results in correspondingly reduced numerical dispersion, and that it also leads (beyond a relatively low threshold) to a significant decrease in computational effort to attain a prescribed accuracy. Finally, we have also demonstrated that this new approach can be easily and efficiently parallelized, and we presented a number of fully three-dimensional calculations that illustrate its almost optimal scalability.

ACKNOWLEDGMENT

This work was supported in part by the Army High Performance Computing Research Center (AHP CRC) under Army Research Laboratory cooperative agreement number DAAD19-01-2-0014. FR also gratefully acknowledges support from AFOSR through contract No. FA9550-05-1-0019 and from NSF through grant No. DMS-0311763. The computations for this project were carried out at the Minnesota Supercomputing Institute, whose support is also gratefully acknowledged.

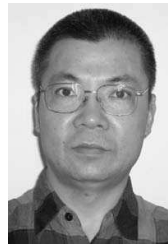
DISCLAIMER

Effort sponsored by AHP CRC under the auspices of the Department of the Army, Army Research Laboratory cooperative agreement number DAAD19-01-2-0014 and by the Air Force Office of Scientific Research, Air Force Materials Command, USAF, under grant number FA9550-05-1-0019. The US Government is authorized to reproduce and distribute reprints for governmental purposes notwithstanding any copyright notation thereon. The views and conclusions contained herein are those of the author and should not be interpreted as necessarily representing the official policies or endorsements, either expressed or implied, of the Air Force Office of Scientific Research, the Army Research Laboratory or the US Government.

REFERENCES

- [1] M. Krumpolz and L. Katehi, "MRTD: New time-domain schemes based on multiresolution analysis," *IEEE Trans. Microwave Theory Tech.*, vol. 44, no. 4, pp. 555–571, Apr 1996.
- [2] K. S. Yee, "Numerical solution of initial boundary value problems involving Maxwell's equations in isotropic media," *IEEE Trans. Antennas Propagat.*, vol. AP-14, no. 3, pp. 302–307, May 1966.
- [3] R. F. Harrington, *Field Computation by Moment Methods*. New York, NY: Macmillan, 1968.
- [4] I. Daubechies, *Ten Lectures on Wavelets*, ser. CBMS-NSF Lecture Notes. Philadelphia, PA: SIAM, 1992, vol. 61.
- [5] X. Zhu, L. Carin, and T. Dogaru, "Parallel implementation of the biorthogonal multiresolution time-domain method," *Journal of the Optical Society of America A*, vol. 20, no. 5, pp. 844–855, May 2003.
- [6] C. D. S. K. Tomko, P. Czarnul, S.-H. Hung, R. L. Robertson, D. Chun, E. S. L. Davidson, and L. P. B. Katehi, "Multiresolution time domain modeling for large scale wireless communication problems," in *IEEE Antennas and Propagat. Soc. Int. Symposium*, vol. 3, Boston, MA, July 2001, pp. 557–560.
- [7] E. M. Tentzeris, R. L. Robertson, J. F. Harvey, and L. P. B. Katehi, "Stability and dispersion analysis of Battle-Lemarie-based MRTD schemes," *IEEE Trans. Microwave Theory Tech.*, vol. 47, no. 7, pp. 1004–1013, Jul 1999.
- [8] M. Fujii and W. J. R. Hofer, "Numerical dispersion in Haar-wavelet based MRTD scheme – comparison between analytical and numerical results," in *Proc. 15th Annu. Rev. Progr. Appl. Comput. Electromagn.*, vol. 1, Monterey, CA, Mar 1999, pp. 602–607.
- [9] S. Grivet-Talocia, "On the accuracy of Haar-based multiresolution time-domain schemes," *IEEE Microwave Guided Wave Lett.*, vol. 10, no. 10, pp. 397–399, Oct 2000.
- [10] T. Dogaru and L. Carin, "Multiresolution time-domain using CDF biorthogonal wavelets," *IEEE Trans. Microwave Theory Tech.*, vol. 49, no. 5, pp. 902–912, May 2001.
- [11] C. D. Sarris and L. P. B. Katehi, "Fundamental gridding-related dispersion effects in multiresolution time-domain schemes," *IEEE Trans. Microwave Theory Tech.*, vol. 49, no. 12, pp. 2248–2257, Dec 2001.
- [12] T. Dogaru and L. Carin, "Scattering analysis by the multiresolution time-domain method using compactly supported wavelet systems," *IEEE Trans. Microwave Theory Tech.*, vol. 50, no. 7, pp. 1752–1760, Jul 2002.

- [13] Y. A. Hussein and S. M. El-Ghazaly, "Extending multiresolution time-domain (MRTD) technique to the simulation of high-frequency active devices," *IEEE Trans. Microwave Theory Tech.*, vol. 51, no. 7, pp. 1842–1851, Jul 2003.
- [14] E. M. Tentzeris, R. L. Robertson, and L. P. B. Katehi, "PML implementation for the Battle-Lemarie multiresolution time-domain schemes," in *Proc. 14th Annu. Rev. Progr. Appl. Comput. Electromagn.*, vol. 2, Monterey, CA, Mar 1998, pp. 647–654.
- [15] Y. W. Cheong, Y. M. Lee, K. H. Ra, J. G. Kang, and C. C. Shin, "Wavelet-Galerkin Scheme of Time-Dependent Inhomogeneous Electromagnetic Problems," *IEEE Microwave Guided Wave Lett.*, vol. 9, no. 8, pp. 297–299, Aug 1999.
- [16] N. Kovvali, W. Lin, and L. Carin, "Image technique for multiresolution time-domain using nonsymmetric basis functions," *Microwave and Opt. Technol. Lett.*, vol. 47, no. 1, pp. 44–47, Oct 2005.
- [17] Z. Chen and J. Zhang, "Efficient eigen-based spatial-MRTD method for computing resonant structures," *IEEE Microwave Guided Wave Lett.*, vol. 9, no. 9, pp. 333–335, Sep 1999.
- [18] T. Dogaru and L. Carin, "Time-domain sensing of targets buried under a Gaussian, exponential, or fractal rough interface," *IEEE Trans. Geosci. Remote Sensing*, vol. 39, no. 8, pp. 1807–1819, Sep 2001.
- [19] N. Bushyager, E. Dalton, and E. M. Tentzeris, "Modelling of complex RF/wireless structures using computationally optimized time-domain techniques," *Int. J. Numer. Model.*, vol. 17, no. 3, pp. 223–236, May/Jun 2004.
- [20] X. Zhu and L. Carin, "Application of the biorthogonal multiresolution time-domain method to the analysis of elastic-wave interactions with buried targets," *IEEE Trans. Geosci. Remote Sensing*, vol. 42, no. 7, pp. 1502–1511, Jul 2004.
- [21] Y. Chen, Q. Cao, and R. Mittra, *Multiresolution Time Domain Scheme for Electromagnetic Engineering*, ser. Series in Microwave and Optical Engineering. Hoboken, NJ: Wiley-Interscience, 2005, vol. 1.
- [22] J. Zhang and Z. Chen, "Low-dispersive super high-order FDTD schemes," in *Proc. IEEE Antennas and Propagat. Soc. AP-S Int. Symp.*, vol. 3, Salt Lake City, UT, Jul 2000, pp. 1510–1513.
- [23] D. W. Zingg, "Comparison of high-accuracy finite-difference methods for linear wave propagation," *SIAM J. Sci. Comput.*, vol. 22, no. 2, pp. 476–502, 2000.
- [24] M. D. White and M. R. Visbal, "Implicit high-order generalized coordinate solution of Maxwell's equations," in *Proc. IEEE Antennas and Propagat. Soc. AP-S Int. Symp.*, vol. 3, San Antonio, TX, Jun 2002, pp. 256–259.
- [25] S. Zhao and G. W. Wei, "High-order FDTD methods via derivative matching for Maxwell's equations with material interfaces," *J. Comput. Phys.*, vol. 200, no. 1, pp. 60–103, Oct 2004.
- [26] S. E. Sherer and M. R. Visbal, "Time-domain scattering simulations using a high-order overset-grid approach," in *Proc. Computational Electromagnetics in Time-Domain, 2005*, Sep 2005, pp. 44–47.
- [27] K. L. Shlager and J. B. Schneider, "Comparison of the dispersion properties of higher order FDTD schemes and equivalent-sized MRTD schemes," *IEEE Trans. Antennas Propagat.*, vol. 52, no. 4, pp. 1095–1104, Apr 2004.
- [28] E. M. Tentzeris, R. L. Robertson, L. P. B. Katehi, and A. Cangellaris, "Space- and time-adaptive gridding using MRTD technique," in *1997 IEEE MTT-S Int. Microwave Symp. Dig.*, vol. 1, Denver, CO, June 1997, pp. 337–340.
- [29] E. M. Tentzeris, A. Cangellaris, L. P. B. Katehi, and J. Harvey, "Multiresolution time-domain (MRTD) adaptive schemes using arbitrary resolutions of wavelets," *IEEE Trans. Microwave Theory Tech.*, vol. 50, no. 2, pp. 501–516, Feb 2002.
- [30] N. Bushyager and E. M. Tentzeris, "Haar-MRTD time and space adaptive grid techniques for practical RF structures," in *2005 IEEE MTT-S Int. Microwave Symp. Dig.*, Long Beach, CA, June 2005, pp. 1123–1126.
- [31] F. Reitich, "Signature modeling for advanced hardware assessment and design," *Bulletin of the Army High Performance Computing Research Center (AHPCRC)*, vol. 15, no. 1, pp. 15–18, 2005.
- [32] C. D. Sarris, "New concepts for the Multiresolution Time Domain (MRTD) analysis of microwave structures," in *Proc. 34th European Microwave Conf.*, vol. 2, London, United Kingdom, Oct 2004, pp. 881–884.
- [33] S. Gottlieb, C.-W. Shu, and E. Tadmor, "Strong stability-preserving high-order time discretization methods," *SIAM Rev.*, vol. 43, no. 1, pp. 89–112, 2001.
- [34] M.-H. Chen, B. Cockburn, and F. Reitich, "High-order RKDG methods for computational electromagnetics," *J. Sci. Comput.*, vol. 22/23, no. 1-3, pp. 205–226, Jun 2005.
- [35] G. Strang, "Wavelets and dilation equations: a brief introduction," *SIAM Rev.*, vol. 31, no. 4, pp. 614–627, Dec 1989.
- [36] B. Cockburn, "Discontinuous Galerkin methods for convection-dominated problems," in *High-Order Methods for Computational Physics*, ser. Lecture Notes in Computational Science and Engineering, T. Barth and H. Deconink, Eds. Berlin: Springer Verlag, 1999, vol. 9, pp. 69–224.
- [37] B. Cockburn and C.-W. Shu, "Runge-Kutta discontinuous Galerkin methods for convection-dominated problems," *J. Sci. Comput.*, vol. 16, no. 3, pp. 173–261, Sep 2001.



Qunsheng Cao received his Ph.D. in electrical engineering from The Hong Kong Polytechnic University in 2001. From 2001 to 2005 he worked as a Research Associate in the Department of Electrical Engineering, University of Illinois at Urbana-Champaign and at the Army High Performance Computing Research Center (AHPCRC), University of Minnesota. In 2005, Dr. Cao joined Nanjing University of Aeronautics and Astronautics (NUAA), China, as a Professor of electrical engineering. Dr. Cao's current research interests are in computational electromagnetics, and particularly in time-domain numerical techniques (FDTD, MRTD and TDFEM) for the study of microwave devices and scattering applications. Dr. Cao has published more than thirty papers in refereed journals and conference proceedings and he is a co-author of the book *Multiresolution Time Domain Scheme for Electromagnetic Engineering* (Series in Microwave and Optical Engineering, vol. 1, Wiley, 2005).



Ramdev Kanapady received his Ph.D. degree in mechanical engineering from the University of Minnesota, Twin Cities, in 2001. From 2001 to 2003 he continued his tenure as Research Associate in the Department of Mechanical Engineering. From 2003 to 2005 he was research scientist and technology transfer scientist at the Army High Performance Computing Research Center (AHPCRC) and continued as Affiliate Graduate Faculty at the Department of Mechanical Engineering, University of Minnesota. His research interests are in the areas of computational mechanics and high performance computing in multidisciplinary/interdisciplinary fields.



Fernando Reitich received his Ph.D. degree in mathematics from the University of Minnesota, Twin Cities, in 1991. From 1991 to 1994 he was a Zeev Nehari Assistant Professor in the Department of Mathematics at Carnegie Mellon University in Pittsburgh, PA. From 1994 to 1997 Dr. Reitich was Assistant and then Associate Professor at North Carolina State University. In 1997, he joined the School of Mathematics at the University of Minnesota, where he is currently Professor. His current research interests are broadly in the area of computational electromagnetics. Dr. Reitich is currently the Associate Director of the Minnesota Center for Industrial Mathematics (MCIM), and he also serves as Portfolio Coordinator for the Battlefield Environment Portfolio at the Army High Performance Computing Research Center (AHPCRC).